

Research Article

Youchun Zou, Chao Xiong*, and Junhui Yin

Experimental and microstructure analysis of the penetration resistance of composite structures

<https://doi.org/10.1515/secm-2021-0036>

received May 10, 2021; accepted June 24, 2021

Abstract: Composite structures (SiC/UHMWPE/TC4; SiC/TC4/UHMWPE) were designed using silicon carbide (SiC) ceramics, ultra-high-molecular-weight polyethylene (UHMWPE) laminate, and titanium alloys (TC4s). Penetration experiments and numerical simulations were carried out to study the anti-penetration mechanism and energy characteristics of the composite structures, and the microstructure of the TC4 was analyzed. The results show that the two composite structures designed have advantages in reducing mass and thickness. The energy proportion of the TC4 is the largest among the three materials, which mainly determines the anti-penetration performance. The microstructure of the TC4 in composite structure I shows rough edges of bullet holes, a large number of adiabatic shear bands (ASBs), ASB bends and bifurcates, and many cracks, which lead to spalling damage of the TC4. The microstructure of the TC4 in composite structure II shows flat edges of bullet holes, several straight ASBs, and no cracks, which leads to brittle fragmentation. The initiation, expansion, combination of ASBs and cracks lead to more energy consumption. Therefore, the combination form of composite structure I can give full play the energy dissipation mechanism of the TC4 and has better anti-penetration performance than composite structure II.

Keywords: armor, anti-penetration, finite element simulation, adiabatic shear band

1 Introduction

The development of anti-armor weapons poses an increasing threat to armored vehicles. Countries around the world are

committed to improving the anti-penetration performance of armored structures [1]. In addition, since the design of armor structure needs to consider lightweight, the lightweight anti-penetration structure is one of the research hotspots in the field of protection [2]. The multilayer composite structure composed of lightweight materials can give full play the physical properties of different materials through reasonable configuration and has good anti-penetration performance, which has attracted wide attention.

The materials used in the multilayer composite anti-penetration structures mainly include ceramics, metal alloys, and fiber composite materials [3,4]. The widely used forms of anti-penetration structures include ceramic-metal, ceramic-fiber composite materials, and metal-fiber composite materials. An et al. [5] studied the anti-penetration performance of ceramic-metal structures, and it is found that the metal has a significant influence on the damage characteristics of the composite structures. The ceramic-metal composite structure has advantages in reducing the thickness and mass of the composite protective structure. Based on the excellent anti-penetration performance of the ceramic-metal composite armor, scholars have conducted in-depth research on it. Tan et al. [6] analyzed the influence of the cover plate on the armor failure mechanism and found that the cover plate effectively reduces the speed of the projectile and the damage of the metal support plate. In addition, the anti-penetration of the ceramic-metal composite structure is also affected by the adhesive layer. Gao et al. [7] studied the influence of the adhesive layer on the anti-penetration performance of the ceramic-metal structure through experiments and numerical. The results show that the increase in the thickness of the adhesive layer leads to a reduction in the size of the ceramic fracture and an increase in the energy absorption capacity of the material. Hu et al. [8] designed the SiC/UHMWPE composite armor and conducted penetration tests. The experimental results showed that the structural form of the hard faceplate and the flexible support plate has guiding significance for the design of the light armor. Cai et al. [9] conducted an experimental study on the failure mechanism of the aluminum foam/UHMWPE composite structure under the combined loading of explosion

* **Corresponding author: Chao Xiong**, Department of Artillery Engineering, Army Engineering University of PLA, Shijiazhuang 050003, China, e-mail: ljgcdxxiongchao@163.com

Youchun Zou, Junhui Yin: Department of Artillery Engineering, Army Engineering University of PLA, Shijiazhuang 050003, China

Table 1: Designed composite structures

Structure number	Arrangement form
I	5 mm SiC/5 mm UHMWPE/6 mm TC4
II	5 mm SiC/6 mm TC4/5 mm UHMWPE

and fragments. The results showed that the UHMWPE laminate in the composite structure can be beneficial to improve the comprehensive protection ability.

At present, there are a few research studies on the anti-penetration mechanism of the multilayer composite structures of three or more materials. In addition, studies have shown that the microstructure has a great influence on the penetration resistance of metal materials [10]. Most studies focus on single-layer metal materials [11–13], and there are a few research studies on the damage mechanism and microstructure of metal materials in composite structures. In this study, two composite structures (SiC/UHMWPE/TC4; SiC/TC4/UHMWPE) were designed using silicon carbide (SiC) ceramics, ultra-high-molecular-weight polyethylene (UHMWPE) laminate, and titanium alloys (TC4s). First,

the anti-penetration mechanism of the composite structures was studied through penetration experiments. Then, the energy characteristics of the composite structures were investigated through numerical methods. Finally, the microstructures of the TC4 were analyzed.

2 Materials and methods

2.1 Materials

The materials used to prepare the composite structures include SiC ceramics, UHMWPE laminate, and TC4s. The thicknesses of SiC ceramics, UHMWPE laminate, and TC4s are 5, 5, and 6 mm, respectively. Based on the reasonable combination forms of the composite protection structures, the composite structures in Table 1 were designed. SiC ceramics is usually used as the panel of composite structures due to its high hardness and high strength. However, SiC ceramics is fragile and has low tensile strength, and so, it

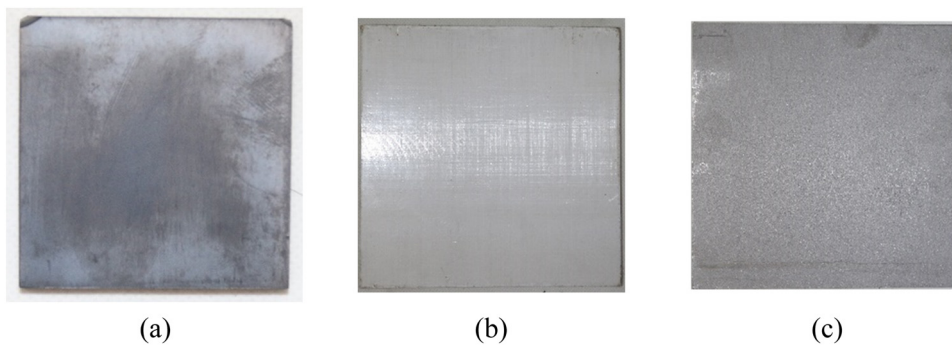


Figure 1: (a) SiC ceramics; (b) UHMWPE laminates; and (c) TC4.

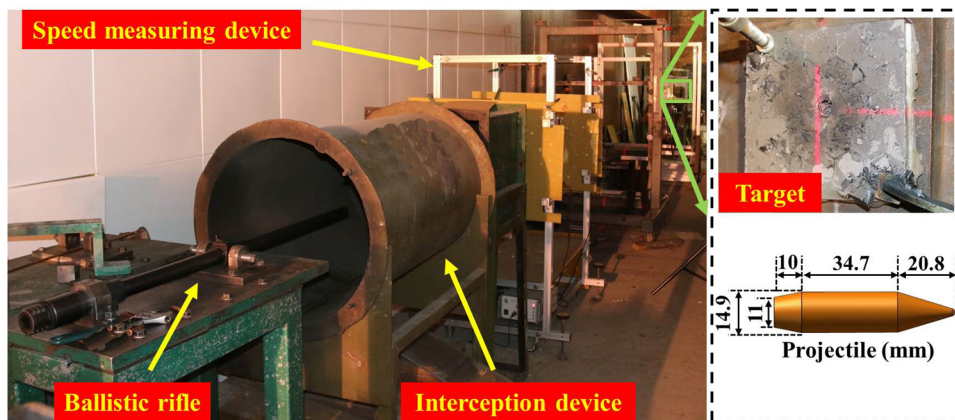


Figure 2: Experimental device for the penetration test.

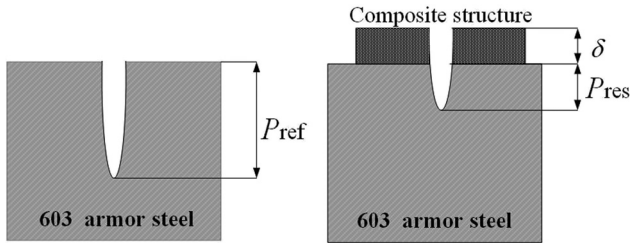


Figure 3: Schematic of the DOP method.

needs to be used in combination with other materials. UHMWPE has a high specific strength and specific modulus, which can resist impact and consume residual energy. TC4 can further improve the protective performance in the composite structure. As shown in Table 1, UHMWPE laminate and TC4 are placed in different positions to discuss the influence of the material arrangement on the anti-penetration performance of composite structures. The interfaces between the materials were bonded with epoxy resin. As shown in Figure 1, based on the experimental device, the cross-sectional size of the composite structures in the penetration test is 150 mm × 150 mm.

2.2 Methods

2.2.1 Penetration test

The experimental device for the penetration test is shown in Figure 2. The ballistic rifle is used to fire projectiles.

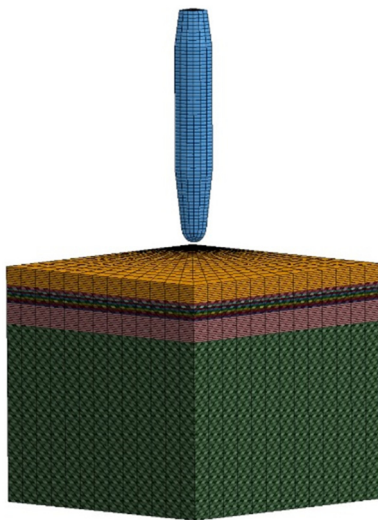


Figure 4: Finite element model.

The material of the projectile is T12A steel, and the dimensions are as shown in the figure. The composite structures to be tested are constrained on the restraint device. The speed measuring device is used to measure the initial velocity of the projectile. An interception device is installed between the ballistic rifle and the speed measuring device.

The depth of penetration (DOP) method was used to evaluate the anti-penetration performance of the composite structures. As shown in Figure 3, 603 armor steel was placed behind the composite structure in the DOP method. The mass efficiency F_m and thickness efficiency F_S of the composite structures are calculated by measuring the residual penetration depth P_{res} and the reference penetration depth P_{ref} of the 603 armor steel. In order to ensure the accuracy of the test results, three samples were prepared for each structure, and the valid value of the three test results was taken. The F_m and F_S are calculated as follows [5,14]:

$$F_m = \frac{(P_{ref} - P_{res}) \cdot \rho_{603}}{\delta \cdot \rho_{hs}} \quad (1)$$

$$F_S = \frac{P_{ref} - P_{res}}{\delta} \quad (2)$$

where P_{ref} is the DOP in 603 armor steel without the composite structure, P_{res} is the residual DOP in 603 armor steel by the projectile penetrated through the composite structure, ρ_{603} is the density of 603 armor steel, δ is the thickness of the composite structure, and ρ_{hs} is the average density of the composite structure. P_{ref} is 43 mm and ρ_{603} is 7.86 g/cm³.

Table 2: *MAT_JOHNSON_HOLMQUIST_CERAMICS [15] constants for SiC ceramics

Constants	SiC ceramics
Density, (g/cm ³)	3.2
Shear modulus, G (GPa)	183
Intact strength coefficient, A	0.96
Fracture strength coefficient, B	0.35
Strain rate coefficient, C	0.0045
Intact strength exponent, N	0.65
Fracture strength exponent, M	1
Maximum tensile pressure strength, T (GPa)	0.75
Pressure at HEL, PHEL (GPa)	14.567
Damage coefficient, D_1	0.48
Damage exponent, D_2	0.48
Bulk modulus, K_1 (GPa)	217.2
Pressure coefficient, K_2 (GPa)	0
Pressure coefficient, K_3 (GPa)	0

Table 3: *MAT_COMPOSITE_DAMAGE [16] constants for UHMWPE laminate

Constants	UHMWPE laminate
Density, (g/cm ³)	0.97
Young's modulus in the <i>a</i> -direction, E_a (GPa)	29.8
Young's modulus in the <i>b</i> -direction, E_b (GPa)	29.8
Young's modulus in the <i>c</i> -direction, E_c (GPa)	1.91
Poisson's ratio, <i>ba</i> ν_{ba} (GPa)	0.008
Poisson's ratio, <i>ca</i> ν_{ca} (GPa)	0.044
Poisson's ratio, <i>cb</i> ν_{cb} (GPa)	0.044
Shear modulus, <i>ab</i> G_{ab} (GPa)	0.82
Shear modulus, <i>bc</i> G_{bc} (GPa)	0.75
Shear modulus, <i>ca</i> G_{ca} (GPa)	0.75
Bulk modulus of the failed material, K_{fail} (GPa)	2.2
AOPT	0
Material axes change flag (MACF) for brick elements	1
Shear strength, S_c (GPa)	0.36
Longitudinal tensile strength, <i>a</i> -axis, X_t (GPa)	3
Transverse tensile strength, <i>b</i> -axis, Y_t (GPa)	3
Transverse compressive strength, <i>b</i> -axis, Y_c (GPa)	2.5
Shear stress parameter for the nonlinear term, α	0.5
Normal tensile strength, S_n (GPa)	0.95
Transverse shear strength, S_{yz} (GPa)	0.95
Transverse shear strength, S_{xz} (GPa)	0.95

2.2.2 Numerical simulation

The LSDYNA finite element software was used to simulate the penetration process of the composite structures. Due to the symmetry of the system and in order to simplify the calculation, a quarter model was established. The geometric parameters of the finite element model are consistent with those of the experiment. The UHMWPE laminate is made of 10 layers of fibers by hot pressing. The ply

structure of the UHMWPE laminate was established in the model to reflect the deformation characteristics in the process of penetration. The boundaries of the composite structure were fully constrained. The mesh size of the projectile is 1 mm. In the penetration test, the deformation and damage of the composite structures were mainly concentrated near the impact point, and the deformation in the rest of the area was not obvious. The mesh of the composite structure was refined within twice the radius

Table 4: *MAT_JOHNSON_COOK [15] constants for the TC4

Constants	TC4
Density, (g/cm ³)	4.45
Shear modulus, G (GPa)	41.9
Static yield strength, A (GPa)	1
Strain hardening coefficient, B (GPa)	0.845
Strain hardening exponent, n	0.58
Strain rate coefficient, C	0.014
Reference strain rate, $\dot{\epsilon}_0$ (s ⁻¹)	1
Thermal softening exponent, m	0.753
Reference temperature, t_0 (K)	298
Melting temperature, t_m (K)	1,951
Damage constant, D_1	0.05
Damage constant, D_2	0.27
Damage constant, D_3	-0.48
Damage constant, D_4	0.014
Damage constant, D_5	3.8

Table 5: *MAT_JOHNSON_COOK [15] constants for the projectile

Constants	T12A steel
Density, (g/cm ³)	7.85
Shear modulus, G (GPa)	200
Static yield strength, A (GPa)	1.54
Strain hardening coefficient, B (GPa)	0.477
Strain hardening exponent, n	0.26
Strain rate coefficient, C	0
Reference strain rate, $\dot{\epsilon}_0$ (s ⁻¹)	1
Thermal softening exponent, m	1
Reference temperature, t_0 (K)	298
Melting temperature, t_m (K)	1,763
Damage constant, D_1	2
Damage constant, D_2	0
Damage constant, D_3	0
Damage constant, D_4	0
Damage constant, D_5	0

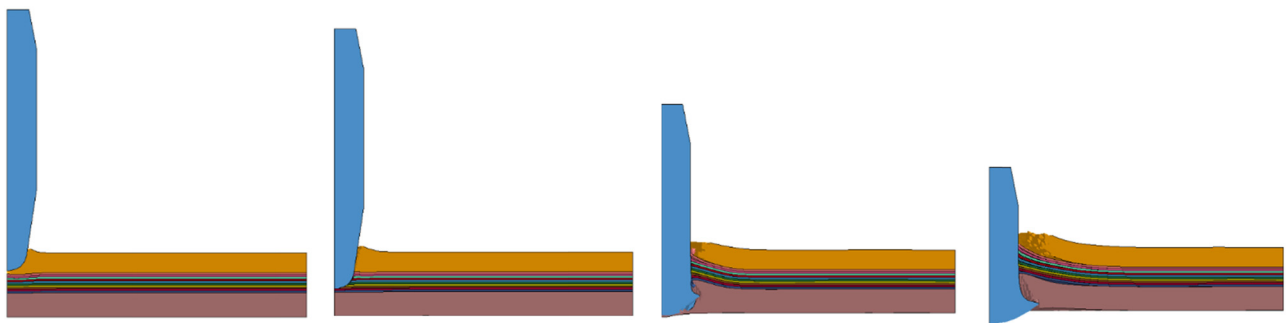
Table 6: *MAT_JOHNSON_COOK [5] constants for 603 armor steel

Constants	603 steel
Density, (g/cm^3)	7.85
Shear modulus, G (GPa)	77
Static yield strength, A (GPa)	1.41
Strain hardening coefficient, B (GPa)	0.73
Strain hardening exponent, n	0.26
Strain rate coefficient, C	0.014
Reference strain rate, $\dot{\epsilon}_0$ (s^{-1})	5,000
Thermal softening exponent, m	1.03
Reference temperature, t_0 (K)	298
Melting temperature, t_m (K)	1,793
Damage constant, D_1	0.05
Damage constant, D_2	3.44
Damage constant, D_3	-2.12
Damage constant, D_4	0.002
Damage constant, D_5	1.61

of the projectile, and the mesh size is 0.1 mm. The model and mesh are shown in Figure 4. *CONTACT_ERODING_SURFACE_TO_SURFACE was used to define the contact between the projectile and the composite structure. Due to the thin thickness of epoxy resin, *CONTACT_TIED_SURFACE_TO_SURFACE was used to define the adhesive. The failure tensile stress and the failure shear stress of the epoxy resin were set to 120 and 80 MPa, respectively [15]. The parameters of the material models are shown in Tables 2–6.

Table 7: Experimental and numerical results

Structure number	Incident velocity (m/s)	ρ_{hs} (g/cm^3)	δ (mm)	P_{res} (mm)		
				Experiment	Numerical	Error (%)
I	980.4	2.76	17.4	6.64	5.94	-10.5
II	983.8	2.64	18.3	7.17	6.94	-3.2

**Figure 5:** Penetration process of composite structure I.

3 Results and discussion

3.1 Analysis of the anti-penetration mechanism

As shown in Table 7, the experiment and simulation results give good agreement, and the anti-penetration mechanism of the composite structures can be further studied through the established model.

The penetration process of composite structure I is shown in Figure 5. In the process of penetrating the SiC ceramics, the projectile deforms plastically and the SiC fractures. With projectile further penetration, the projectile penetrates the UHMWPE laminate. The failure morphology of the UHMWPE laminate is shown in Figure 6(a). The UHMWPE fiber first undergoes tensile deformation, and shear failure occurs under the penetration of the projectile before the fiber reaches the ultimate tensile strength. The restraint of the TC4 on the UHMWPE laminate leads to the eversion of the UHMWPE fiber on the front surface. The stress wave is reflected as a tensile wave between the matrix and the fiber of the UHMWPE laminate. When the tensile stress is greater than the adhesion between layers, delamination failure occurs. The failure morphology of the TC4 is shown in Figure 6(b). The failure mode of TC4 is spalling damage. Due to the high strength and hardness of the TC4, the projectile is further damaged inside the TC4.

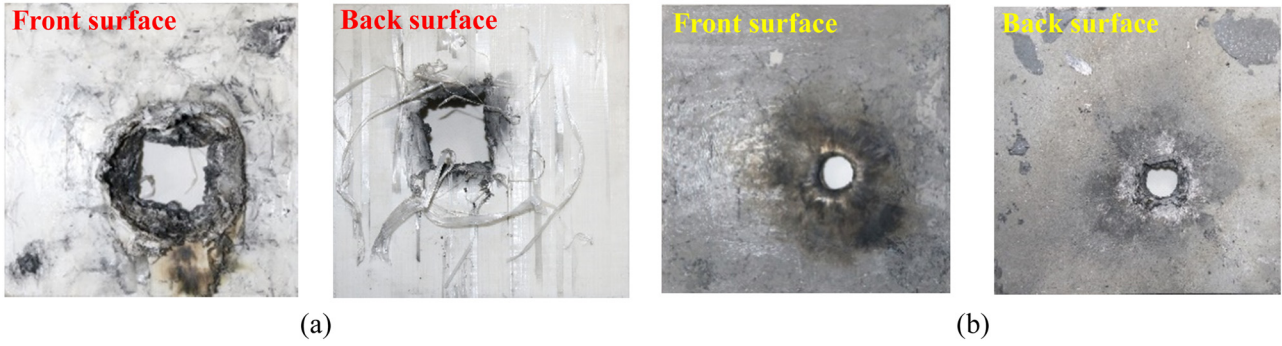


Figure 6: Failure morphology of (a) the UHMWPE laminate and (b) TC4.

The penetration process of composite structure II is shown in Figure 7. The failure morphology of the TC4 is shown in Figure 8(a). The failure mode of the TC4 in composite structure II is brittle fragmentation. TC4 undergoes shear failure first, and the brittle fragmentation occurs as the projectile further pushes the TC4. The failure morphology of the UHMWPE laminate is shown in Figure 8(b). The failure mode of the UHMWPE laminate in

composite structure II is a shear failure, and there is a certain degree of tensile failure on the front surface. In composite structure II, the UHMWPE laminate is the backplate of TC4. After the projectile penetrates TC4, the projectile and TC4 fragments form a combined projectile to penetrate the UHMWPE laminate. The UHMWPE laminate has low strength and stiffness, and shear failure occurs under the combined penetration of projectiles and

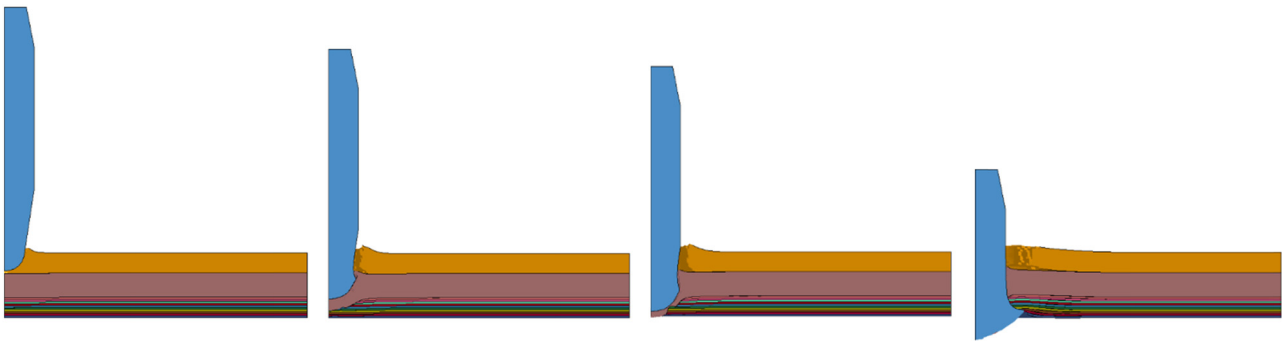


Figure 7: Penetration process of composite structure II.

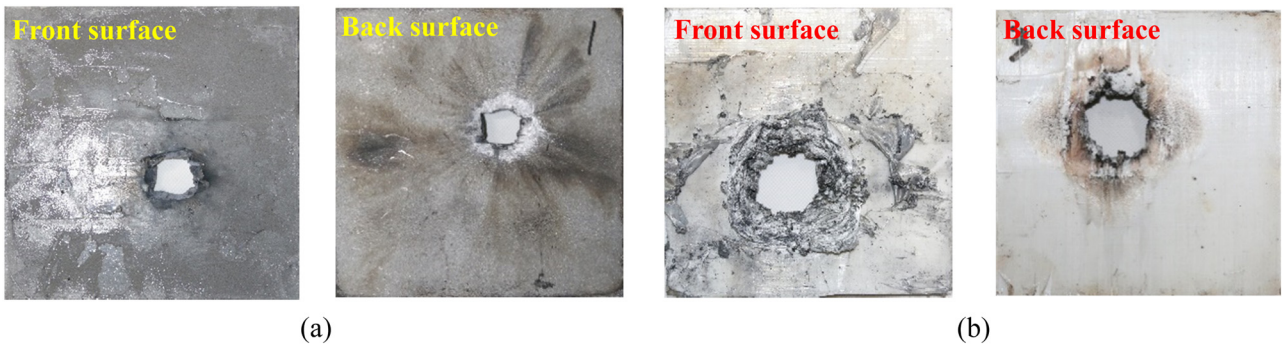


Figure 8: Failure morphology of (a) TC4 and (b) the UHMWPE laminate.

Table 8: The mass efficiency and thickness efficiency of composite structures

Structure number	Incident velocity (m/s)	ρ_{hs} (g/cm ³)	δ (mm)	P_{res} (mm)	F_m	F_s
I	976.4	2.76	17.4	5.52	6.14	2.15
II	976.4	2.64	18.3	6.24	5.98	2.01

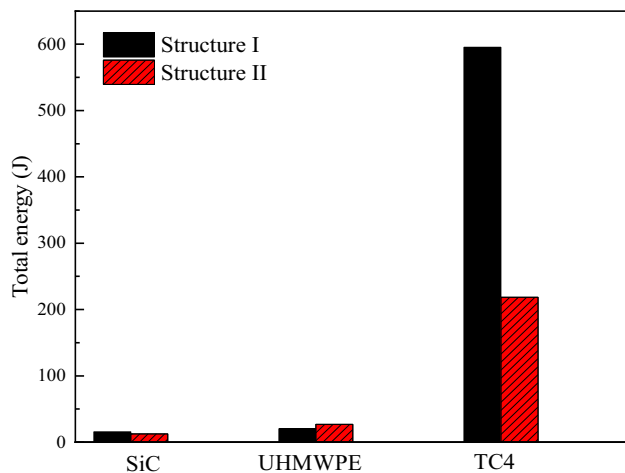
TC4 fragments. The restriction of TC4 leads to a small deformation of the UHMWPE laminate, which is not conducive to exerting the energy absorption performance of the UHMWPE laminate.

3.2 Numerical simulation analysis

As shown in Table 8, in order to compare the protective performance of the composite structures, the mass efficiency F_m and thickness efficiency F_s of the composite structures at the same incident velocity were calculated by numerical methods. The F_m and F_s of the composite

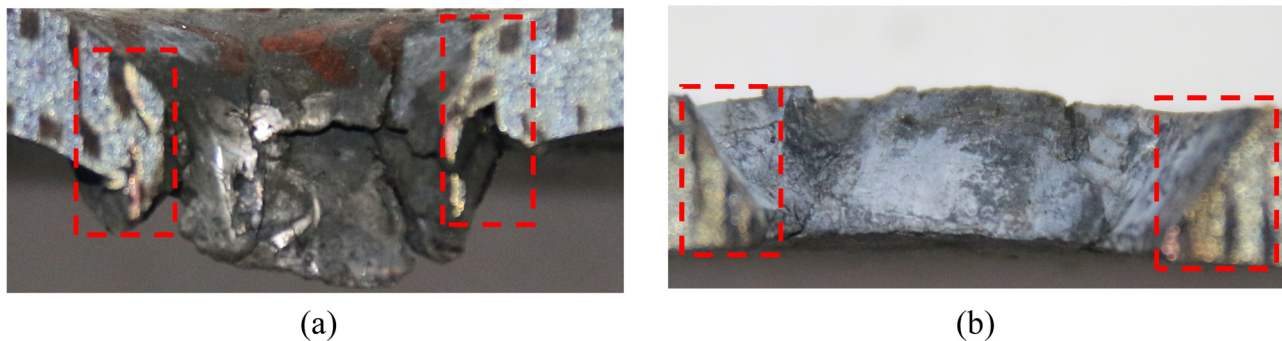
structures are all greater than 1, indicating that the designed composite structures have advantages in reducing mass and thickness. In addition, it can be found that the protective performance of structure I is better.

As shown in Figure 9, the total energy of different materials was calculated by numerical methods. It can be found that the total energy proportion of TC4 is the largest, indicating that TC4 mainly determines the anti-penetration performance of the composite structures. In order to improve the anti-penetration performance of the composite structures, the energy dissipation mechanism of TC4 should be fully utilized. Metal materials such as TC4 mainly rely on their high strength and high hardness to abrade the projectile and consume its energy. The brittle fragmentation of TC4 belongs to a low-energy consumption failure mode, and the spalling damage belongs to a high-energy consumption failure mode. Therefore, the total energy of the TC4 in composite structure I is greater than the total energy of TC4 in composite structure II. TC4 has higher total energy in composite structure I, which indicates that the TC4 can give full play its energy dissipation performance and maximize the anti-penetration performance of composite structure when it is placed behind the UHMWPE laminate.

**Figure 9:** Total energy of different materials.

3.3 Micro-damage features of TC4

It is concluded from Section 3.2 that TC4 has the largest proportion of energy and the most significant impact on

**Figure 10:** Samples used for microstructure analysis: (a) composite structure I and (b) composite structure II.

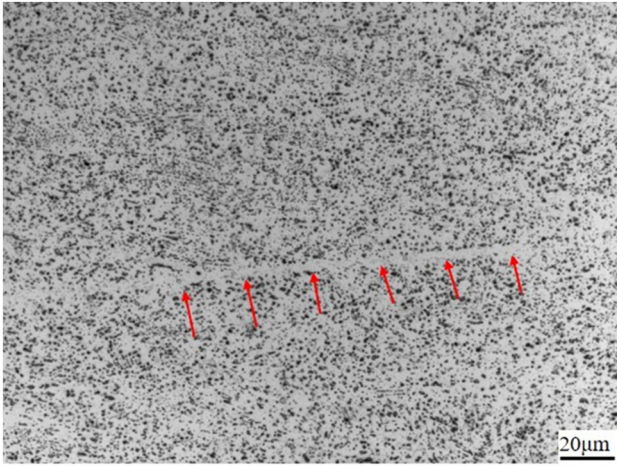


Figure 11: Adiabatic shear bands.

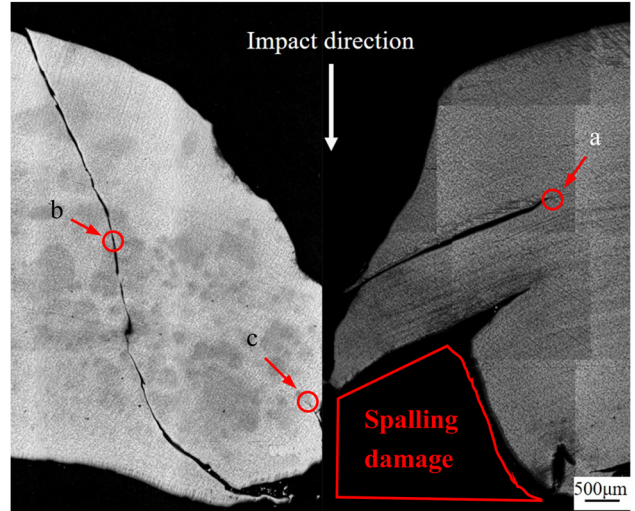
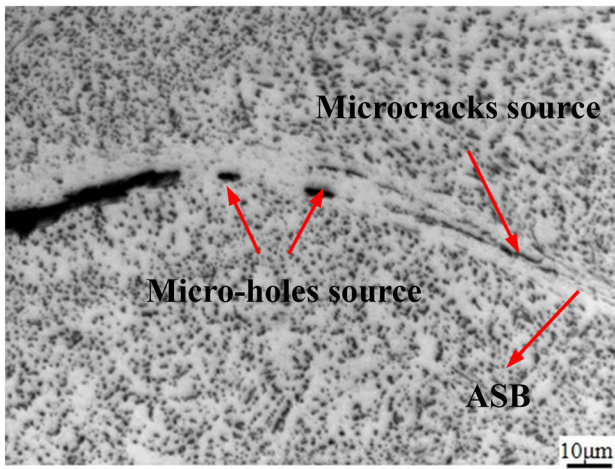
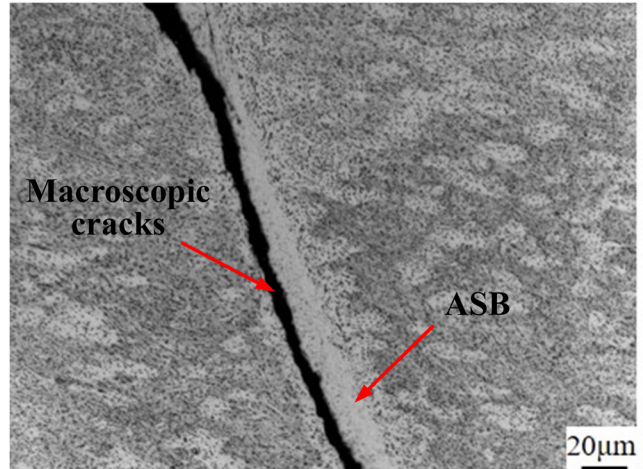


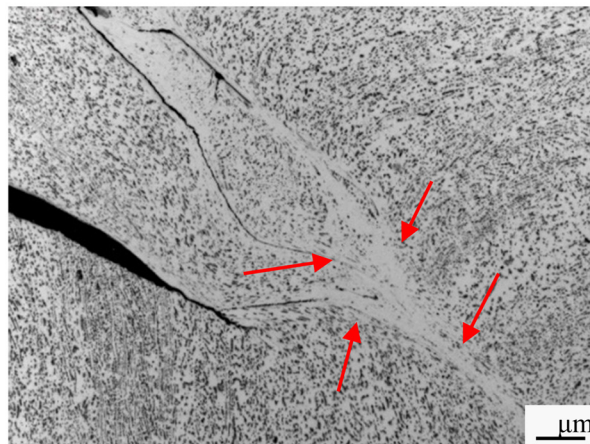
Figure 12: Microstructure of TC4 bullet holes in composite structure I.



(a)



(b)



(c)

Figure 13: ASB in composite structure I: (a) microcrack and microhole sources, (b) macroscopic cracks, and (c) bifurcation of ASB.

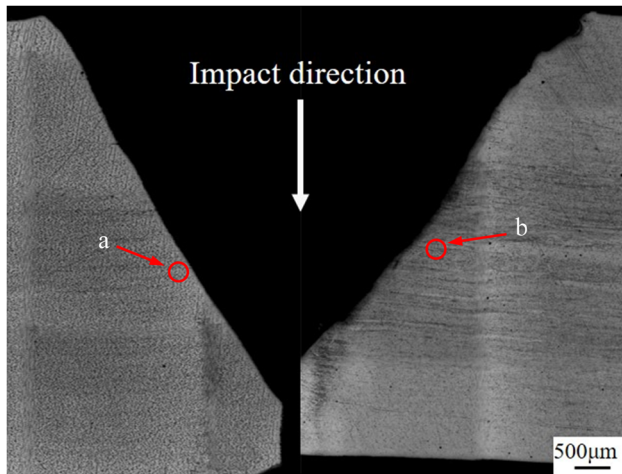


Figure 14: Microstructure of TC4 bullet holes in composite structure II.

the anti-penetration performance of the composite structures. Studies have shown that the failure mechanism of TC4 is closely related to the microstructure characteristics [13]. In order to deeply study the anti-penetration mechanism of the composite structures, the microstructure analysis of the TC4 was carried out. The penetrated TC4 was cut along the midline of the crater, and the samples shown in the dashed box in Figure 10 were cut for microstructure analysis. The observation position is the section near the bullet hole in the dashed box. The samples were ground, polished, and etched with a 2 mL HF + 6 mL HNO₃ + 92 mL H₂O solution for 10–15 s, and examined using an Axiovert-2000MAT optical microscope for microstructure analysis.

TC4 is in a state of high temperature, high pressure, and high strain rate under the penetration of the projectile. Due to the extremely short penetration time, there is no

time for the heat generated inside TC4 to dissipate, causing an adiabatic phenomenon. The adiabatic phenomenon leads to material instability, causing severe plastic deformation in local locations and ASBs are formed. As shown in Figure 11, the tissue morphology of ASBs is different from that of the matrix. The tissue in the ASBs is broken due to shearing, and there is a clear boundary with the matrix tissue.

The microstructure of TC4 samples in composite structure I is shown in Figure 12. It can be found that the edges of the bullet holes are rough, and there are multiple cracks and holes in the TC4, and spalling damage of the TC4 appears. The microstructures at positions a–c are shown in Figure 13. As shown in Figure 13(a), due to the inconsistent deformation of the ASB and the matrix, microcrack and microhole sources appear in the ASB. In Figure 13(b), microcracks and microholes are initiated in the ASBs, and macroscopic cracks are formed after the microcracks and microholes further expand and merge. The ASB in Figure 13(c) is bent and bifurcated, which provides more locations and paths for the initiation of crack sources and hole sources.

The microstructure of TC4 samples in composite structure II is shown in Figure 14. Compared with the TC4 in composite structure I, the TC4 in composite structure II has smoother bullet hole edges without cracks and holes. The microstructures at positions a, b are shown in Figure 15. There are a few ASBs and most of them are straight, and there are no cracks and holes in the ASB.

The initiation, expansion, and merger of ASBs and cracks consume a lot of energy. Therefore, the TC4 in composite structure I consume more energy. The Composite structure I can give full play the energy dissipation mechanism of the TC4, and its anti-penetration performance is better than that of composite structure II.

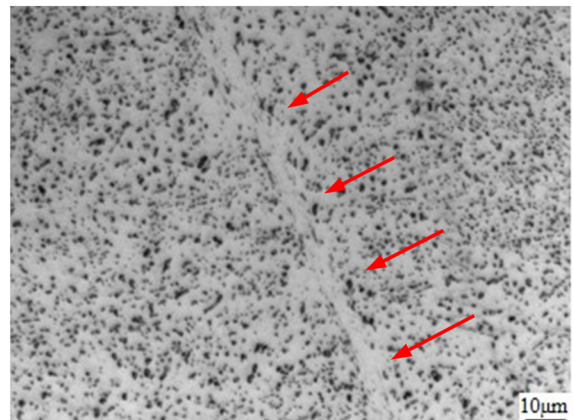
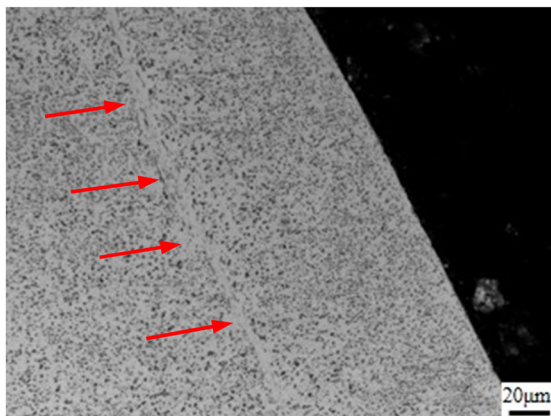


Figure 15: ASB is straight.

4 Conclusions

The penetration tests and numerical simulations were used to study the anti-penetration mechanism and energy characteristics of the composite structures. The failure mode of TC4 was explained based on the microstructure, and the influence of the TC4 microstructure on the anti-penetration performance and energy characteristics was studied. The main conclusions are as follows.

- (1) In the SiC/UHMWPE/TC4 composite structure, the UHMWPE laminate will undergo tensile failure and TC4 will undergo spalling damage. In the SiC/TC4/UHMWPE composite structure, the UHMWPE laminate will undergo shear failure and TC4 will undergo brittle fragmentation. The two composite structures designed have advantages in reducing mass and thickness.
- (2) TC4 has the largest total energy proportion among the three materials and plays an important role in improving anti-penetration performance. The failure mode of the TC4 in composite structure I is spalling damage, which supports fully the energy dissipation mechanism of TC4, and anti-penetration performance is better than that of composite structure II.
- (3) The bullet hole edges of the TC4 in composite structure I are rough, and there are multiple ASBs. ASB bifurcates and generates multiple macroscopic cracks. The bullet holes edges of the TC4 in composite structure II are flat. There are a few ASBs and they are straight without cracks. Since the behavior of ASBs and cracks in composite structure I is more complex, more energy is consumed. The reason for the high-energy consumption of TC4 in composite structure I was explained from the perspective of microstructures.

Conflict of interest: Authors state no conflict of interest.

References

- [1] Fischer H. U.S. Military casualty statistics: operation new dawn, operation Iraqi freedom, and operation enduring freedom. CRS Report for Congress; 2010. p. 12.
- [2] Rawat P, Zhu D, Rahman MZ, Barthelat F. Structural and mechanical properties of fish scales for the bio-inspired design of flexible body armors: a review. *Acta Biomater.* 2021;121:41–67.
- [3] Abtew MA, Boussu F, Bruniaux P, Loghin C, Cristian I. Ballistic impact mechanisms – a review on textiles and fibre-reinforced composites impact responses. *Compos Struct.* 2019;223:110966.
- [4] Crouch IG. Body armour – new materials, new systems. *Def Technol.* 2019;15:241–53.
- [5] An X, Tian C, Sun Q, Dong Y. Effects of material of metallic frame on the penetration resistances of ceramic–metal hybrid structures. *Def Technol.* 2020;16:77–87.
- [6] Tan ZH, Han X, Zhang W, Luo SH. An investigation on failure mechanisms of ceramic/metal armour subjected to the impact of tungsten projectile. *Int J Impact Eng.* 2010;37:1162–9.
- [7] Gao Y, Zhang W, Xu P, Cai X, Fan Z. Influence of epoxy adhesive layer on impact performance of TiB2-B4C composites armor backed by aluminum plate. *Int J Impact Eng.* 2018;122:60–72.
- [8] Hu D, Zhang Y, Shen Z, Cai Q. Investigation on the ballistic behavior of mosaic SiC/UHMWPE composite armor systems. *Ceram Int.* 2017;43:10368–76.
- [9] Cai S, Liu J, Zhang P, Li C, Cheng Y, Chen C. Experimental study on failure mechanisms of sandwich panels with multi-layered aluminum foam/UHMWPE laminate core under combined blast and fragments loading. *Thin-Walled Struct.* 2021;159:107227.
- [10] Zheng C, Wang F, Cheng X, Fu K, Liu J, Wang Y, et al. Effect of microstructures on ballistic impact property of Ti–6Al–4V targets. *Mater Sci Eng A.* 2014;608:53–62.
- [11] Sun K, Yu X, Tan C, Ma H, Wang F, Cai H. Influence of adiabatic shear bands intersection on the ballistic impact of Ti–6Al–4V alloys with three microstructures. *Mater Sci Eng A.* 2014;606:257–67.
- [12] Yu XM, Feng LC, Li GA, He YQ, Qiao B. Impact damage behaviors of Ti–6Al–4V alloy targets with different microstructures. *Mater Sci Eng A.* 2015;639:374–9.
- [13] Zheng C, Wang F, Cheng X, Liu J, Fu K, Liu T, et al. Failure mechanisms in ballistic performance of Ti–6Al–4V targets having equiaxed and lamellar microstructures. *Int J Impact Eng.* 2015;85:161–9.
- [14] Anderson CE, Royal-Timmons SA. Ballistic performance of confined 99.5%-Al₂O₃ ceramic tiles. *Int J Impact Eng.* 1997;19:703–13.
- [15] Tian C, An X, Sun Q, Dong Y. Experimental and numerical analyses of the penetration resistance of ceramic–metal hybrid structures. *Compos Struct.* 2019;211:264–72.
- [16] Wang L, Tang T, Ma J. Numerical simulation of UHMWPE laminated fiber plate resisted projectile. *Appl Mech Mater.* 2013;395–396:24–8.